A bilayer coarse-fine infiltration system minimizes bioclogging: The relevance of depth dynamics

N. Perujo,[a,b,c*] A.M. Romaní,[c] and X. Sanchez-Vila[a,b]

[a] Department of Civil and Environmental Engineering, Universitat Politècnica de Catalunya (UPC), Jordi Girona 1-3, 08034 Barcelona, Spain

[b] Hydrogeology Group (UPC−CSIC), Barcelona, Spain

[c] GRECO - Institute of Aquatic Ecology, Universitat de Girona, 17003 Girona, Spain

*Corresponding author: nuria.perujo.buxeda@gmail.com

Keywords: biofilm attachment/detachment; extracellular polymeric substances (EPS); biofilm activity; porous media; deep clogging, grain size distribution

Abstract

Bioclogging is a main concern in infiltration systems as it may significantly shorten the service life of these low-technology water treatment methods. In porous media, biofilms grow to clog partially or totally the pore network. Dynamics of biofilm accumulation (e.g., by attachment, detachment, advective transport in depth) and their impact on both surface and deep bioclogging are still not yet fully understood. To address this concern, a 104 day-long outdoor infiltration experiment in sand tanks was performed, using secondary treated wastewater and two grain size distributions (GSDs): a monolayer system filled with fine sand, and a bilayer one composed by a layer of coarse sand placed on top of a layer of fine sand. Biofilm dynamics as a function of GSD and depth were studied through cross-correlations and multivariate statistical analyses using different parameters from biofilm biomass and activity indices, plus hydraulic parameters measured at different depths. Bioclogging (both surface and deep) was found more significant in the monolayer fine system than in the bilayer coarse-fine one, possibly due to an early low-cohesive biofilm formation in the former, driven by lower porosity and lower fluxes; under such conditions biomass is favorably detached from the top layer, transported and accumulated in depth, so that new biomass might colonize the surface. On the other hand, in the bilayer system, fluxes are highest, and the biofilm is still in a growing phase, with high microbial activity and low biofilm detachment capability from the top sand layer, resulting in low surface and deep bioclogging. Overall, the bilayer coarse-fine system allows infiltrating higher volume of water per unit of surface area than the monolayer fine one, minimizing surface and deep bioclogging, and thus increasing the longevity and efficiency of infiltration systems.

Graphical abstract

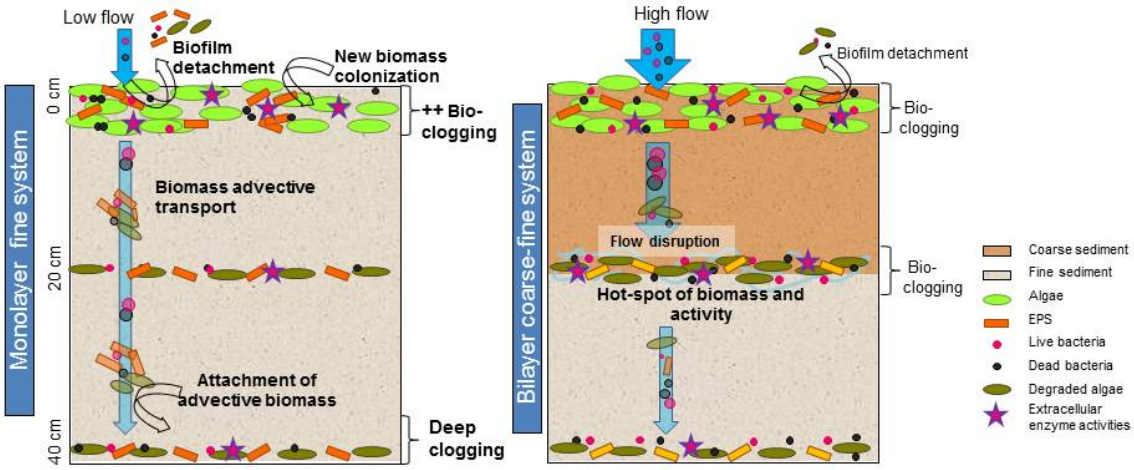

1. Introduction

Infiltration systems are low-tech and low-cost water treatment technologies where the quality of the infiltrated water improves progressively during the infiltration path through the porous medium as a consequence of biological, chemical and physical processes (Dillon et al. 2008; Miller et al. 2009). Infiltration basins are used worldwide for groundwater recharge, wastewater treatment or storm water disposal or reclaim and for setting up hydraulic barriers against the intrusion of undesired (polluted or salinized) water to aquifers (Bardin et al. 2002). Furthermore, they are suitable for the treatment of decentralized sewage (Duan et al. 2015) and have been increasingly used as a way of solving water supply stress problems in urban areas (Camprovin et al. 2017) or reducing the degradation of stream water quality (Türkmen et al. 2008). Simplicity, low capital and low operating costs are the main advantages of infiltration systems compared to more technologically sophisticated water treatment methods (Campos et al. 2002).

Successful performance of infiltration systems relies on the development of biofilm (growth and spatial distribution) within the porous media. Biofilms are recognized to be the dominant mode of bacterial life (Barai et al. 2016). Natural biofilms are mixtures of

56 autotrophic/heterotrophic assemblages (Gette-Bouvarot et al. 2014), composed by algae
57 (microphytobenthos), bacteria, fungi, and protozoa embedded in a matrix of
58 extracellular polymeric substances (EPS) and attached to solid surfaces (Lock et al.
59 1984). EPS constitute a fibrous gel-type matrix which can be broken down into different
60 organic molecules such as polysaccharides, proteins, lipids and nucleic acids (Flemming
61 and Wingender, 2010; Stoodley et al. 2002) and play a crucial role in the initial
62 attachment of cells to solid surfaces, cohesiveness, biofilm thickness (Flemming and
63 Wingender, 2010) and biofilm resistance to external stressors (Flemming et al. 2016).

64 Biofilms play a key role on a number of biogeochemical processes (Mermillod-Blondin
65 et al. 2005; Battin et al. 2016) through uptake, storage, and mineralization of dissolved
66 organic matter, as well as assimilation of inorganic nutrients (Findlay et al. 2003).
67 However, an excessive build-up of microbial biomass -cells and EPS- can cause fouling
68 of the porous media, known as bioclogging (Oberdorfer and Peterson, 1985; Baveye et
69 al. 1998; Thullner, 2010; Zhong and Wu, 2013; Brangarí et al. 2018). Bioclogging
70 reduces the total volume and the connectivity of the pores accessible to flow (Or et al.
71 2007), triggering deleterious consequences on infiltration systems: reducing infiltration
72 efficiency and increasing operating costs (Xia et al. 2014). This limits the availability of
73 oxidants and nutrients to reach the microorganisms (Thullner et al. 2002), affecting the
74 quality of infiltrated waters (Dechesne et al. 2004), creating a highly polluted filter at
75 the top layer (Segismundo et al. 2017), increasing the need for frequent rehabilitation
76 (Bouwer and Rice, 1989), and resulting in untimely system failures (Jeong et al. 2018).
77 In short, bioclogging may significantly shorten the service life of infiltration systems
78 (Duan et al. 2015, Hua et al. 2014).

79 Several works have studied bioclogging processes focusing on the spatial and temporal
80 evolution of bacteria and/or EPS concentrations (Xia et al. 2016; Dupin et al. 2001;

Vandevivere and Baveye, 1992). In outdoor infiltration systems, where biofilms include phototrophs and heterotrophs, the contribution of algae in bioclogging might be also relevant (Gette-Bouvarot et al. 2014), since main producers of EPS are both bacteria and algae (Malarkey et al. 2015; Hirst et al. 2003).

Bioclogging is a complex process (Ding et al. 2018; Zhou et al. 2018; Fu et al. 2013) that includes several biofilm stages: attachment, adhesion, maturation and detachment (Hall-Stoodley et al. 2004). In these stages, the combination of biological parameters and hydraulic stresses, such as unit flow and shear forces, determine bioclogging development by regulating the thickness of the superficial biofilm (Gutiérrez et al. 2018) and the biomass accumulation and removal rate (Kim et al. 2010). Another parameter that plays a key role on bioclogging is the grain size distribution (GSD) of the porous media as it shapes the structure, size distribution and connectivity of the pore network, controlling the functions of the porous media-associated biofilm (Santmire and Leff, 2007). On one hand, GSD defines the surface area available for colonization per unit of sand mass, which increases with decreasing average grain size (Mendoza-Lera et al. 2017). On the other hand, GSD controls hydraulic conductivity (Battin, 2000), largest for coarse sands, allowing large supply of solutes in depth (Higashino, 2013) thus influencing biomass establishment and biofilm activity along the vertical profile (Perujo et al. 2017). As stated by Ding et al. (2018), high biological activity could decrease organic matter accumulation (and the occurrence of bioclogging), but on the other hand it may also enhance biofilm growth which can promote bioclogging. According to de Matos et al. (2018), bioclogging is still a large “black box”, as the main factors that modulate it are not yet well understood.

Two strategies commonly used to control bioclogging are restoration and prevention. The former is based on restoring hydraulic conductivity by replacing the porous media

106 (Nivala et al. 2012) which can be costly, difficult to implement, and not very effective
107 (Tang et al. 2018). In fact, surface clogging (or "cake-clogging") may be reversible
108 (e.g., by scrapping), but this is typically not the case for deep clogging (Pholkern et al.
109 2015). It is therefore necessary to increase our knowledge on bioclogging in order to
110 improve the design and maximize the performance of infiltration media (Farah et al.
111 2016; Duan et al. 2015). In fact, detachment of superficial biofilm and further transport
112 in depth, as well as the growth and attachment of new biomass in depth play a key role
113 in the process of deep bioclogging in infiltration systems. Furthermore, in spite of its
114 importance, few studies have addressed the occurrence of deep clogging (e.g., Gutiérrez
115 et al. 2018; Kia et al. 2018; Segismundo et al. 2017); further, they focused only on
116 physical clogging but not on biological clogging.

117 In this paper, we investigated biofilm growth, detachment and vertical-transport linked
118 to superficial and deep porous media bioclogging by means of statistical correlations
119 and multivariate analysis. In the present study, physical clogging was neglected as
120 infiltrated water used was secondary treated wastewater with low suspended solids
121 concentrations. Specifically, the main objectives of this study are (1) to infer how GSD
122 influence biofilm dynamics (biomass attachment, detachment and interstitial transport)
123 in depth; (2) to improve our ability to control bioclogging by understanding how biofilm
124 dynamics modulate the occurrence of surface and deep clogging as a function of the
125 GSDs, and (3) to disentangle the relationship between biofilm activity and biomass
126 accumulation in the occurrence of bioclogging in infiltration systems. To achieve these
127 objectives, we have compared (i) a system composed by a layer of coarse sand placed
128 on top of another of fine sand, termed bilayer coarse-fine system -as in a previous study
129 Perujo et al. (2017) demonstrated that this setup could result in a hot-spot of biological
130 activity-; and (ii) a system composed by a single layer of fine sand. A complementary

specific objective is to evaluate if the former setup could reduce bioclogging development in infiltration systems.

2. Methodology

2.1. Experimental design

The outdoor infiltration experiment consisted in flow-through sand tanks (0.21 m^3 of capacity) filled following two different setups in terms of grain size distribution: (i) a bilayer system (denoted CF, standing for Coarse-Fine), consisting of a 20 cm layer of coarse sand (0.9 – 1.2 mm) placed on top of a 20 cm layer of fine sand (0.075 – 0.250 mm), in triplicate; and (ii) a monolayer system (denoted F, for Fine), consisting of a 40 cm layer of fine sand (0.075 – 0.250 mm), in triplicate (Fig. 1). Sand porosity (ϕ) was 0.4 for the coarse sand layers and 0.32 for the fine ones.

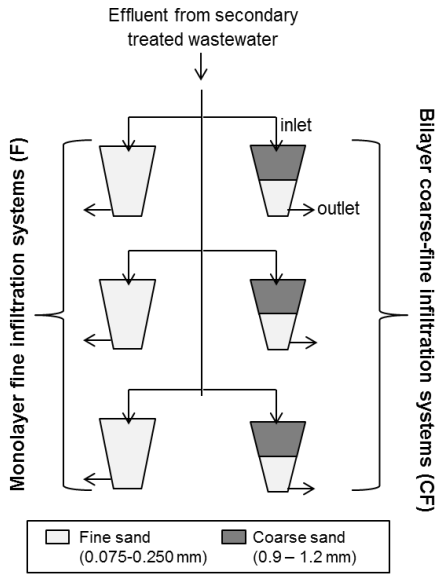

Figure 1 Scheme of the experimental design with two setups (in triplicate) in terms of grain size distribution: (left) monolayer system (F, Fine), with a 40 cm layer of fine sand; (right) bilayer system (CF, Coarse-Fine), 20 cm layer of coarse sand + 20 cm layer of fine sand.

In the upper part of each tank, a valve ensured a constant level of secondary treated wastewater supplied from the Girona urban WWTP (Spain), creating an overlying layer of water and a continuous infiltration resembling vertical flow conditions. A gravel

149 layer was placed at the bottom of each tank to facilitate water drainage towards the
150 outlet. The experiment lasted 104 days (April to July 2016) with a mean outdoor
151 temperature of 21.6 ºC (AEMET – State Agency of Meteorology, Spanish Government)
152 and 234 mm of accumulated rainfall (METEOCAT – Meteorological Service,
153 Government of Catalunya). Sunlight conditions were allowed in the surface of the
154 tanks, to resemble those of real infiltration basins.

155 Three water ports were installed at the wall of each tank, at depths 4, 18 and 38 cm, to
156 measure piezometric head differences (Fig. S1). Piezometric head measurements were
157 taken from day 19 (earlier values could not be recorded due to technical limitations)
158 with 2-4 day intervals, for a total of 26 sampling dates. From these measurements,
159 hydraulic conductivity (K) values were computed corresponding to depth segments
160 limited by contiguous water ports: surface to 5 cm; 5 to 20 cm; 20 to 40 cm, as well as
161 an overall value (surface to 40 cm depth).

162 Sand samplings were performed periodically for a total of 9 sampling dates, always
163 around noon (11 – 12 am), and under similar weather conditions. Sand samples were
164 obtained using a sediment core sampler (Eijkelkamp 04.23.SA) and each core was
165 sliced in three depth layers (0-4 cm denoted as "surface sand", 18-22 cm as "20 cm
166 depth sand", and 36-40 cm as "40 cm depth sand"). Each layer was homogenized, and
167 subsamples of 1 cm^3 were collected using an uncapped syringe, and kept frozen (-20 ºC)
168 until analysis to determine algae (chlorophyll-a) and EPS biomass content. For bacterial
169 density and viability determination, samples were kept at 4 ºC and transported to the
170 laboratory to proceed with the analysis on the same day. Extracellular enzyme activities
171 (EEAs) in the biofilm were measured in fresh on days 47 and 105. After each sand
172 sampling, one methacrylate empty column was placed at all sampling points to avoid
173 sand collapse, in an attempt to minimize the disruption of the flow field.

174 **2.2. Hydraulic conductivity**

175 Hydraulic conductivity, K [in LT^{-1}] was calculated using Darcy's law at the segments
176 already mentioned. For any given two sampling depths, A and B, $K_{(A-B)} = \frac{Q\Delta L_{A-B}}{\Delta hS}$,
177 where Δh is the piezometric head difference between the two points [L], ΔL the length
178 of the depth interval [L], S the cross-section area (= 0.4654 [L^2]), and Q the flow rate
179 [L^3T^{-1}]. K values were calculated at different times, and those corresponding to the first
180 sampling time are indicated as K_0 and reported in Table S1. Values throughout the text
181 are reported normalized by K_0, therefore different for each system.

182 **2.3. Biofilm biomass: Algal biomass (Chlorophyll-a content)**

183 Chlorophyll-a (chl-a) was measured as a proxy for algal biomass. Chl-a concentrations
184 were determined as described by Jeffrey and Humphrey (1975). Acetone 90 % (10 ml)
185 was added to each sand sample to extract chl-a, and samples were kept in the dark for 8-
186 12 h at 4 ºC. Sand samples were sonicated and filtered (GF/C, 1.4 µm, 47 mm).
187 Absorbance was measured at 430, 665 and 750 nm. Results are reported as µg of chl-a ·
188 g dry weight $(DW)^{-1}$. Algal biomass concentrations were also expressed in µg C · g
189 DW^{-1} by using the conversion factor of Chl:C of 0.021 (Li et al. 2010).
190 Complementarily, Margalef pigment index (Margalef, 1983) was calculated from the
191 ratio Abs430/Abs665; the higher the value of Margalef index indicates the higher
192 presence of photosynthetic degraded pigments and thus may indicate algal degradation.

193 **2.4. Biofilm biomass: Content of polysaccharides in EPS**

194 EPS were extracted by a cation exchange resin (CER) which is capable of extracting
195 both colloidal and bound EPS fractions. The content of polysaccharides was measured
196 spectrophotometrically following the protocol described by Dubois et al. (1956). Each
197 individual sample was placed in an Eppendorf with 1 ml of Milli-Q water plus 0.3 g of

198 conditioned CER. After careful shaking, it was incubated with ice for 1 h in a shaker
199 (250 rpm), and then centrifuged (11 000 rpm) for 15 min at 4 ºC. The supernatant (500
200 µl) was pipetted into glass tubes. For each glass tube, a phenol solution (12.5 µl, 80%
201 w/w) was added, shook carefully, followed by an addition of H_2SO_4 (1.25 ml, 95.5%)
202 and capped. After 10 min, samples were carefully shaken and incubated for 10 min in a
203 water bath (30 ºC). Absorbance (485 nm) was measured in a spectrophotometer. Results
204 are given in µg glucose-equivalents·g DW^{-1}. EPS content was also expressed as µg C·g
205 DW^{-1} considering all EPS was built of glucose polysaccharides. Polysaccharides have
206 been proved to be the main component of EPS in sands (Xia et al. 2016; Xia et al. 2014;
207 Hoffmann and Gunkel, 2011).

208 **2.5. Biofilm biomass: Bacterial density and viability**

209 Bacterial density was determined by flow cytometry (FACSCalibur, Becton Dickinson)
210 following a protocol adapted from Amalfitano et al. (2009). Sand samples were placed
211 in glass vials and a detaching solution (10 ml) was added. The detaching solution
212 consists of NaCl (130 mM), Na_2HPO_4 (7mM), NaH_2PO_4 (3mM), formaldehyde (37 %),
213 sodium pyrophosphate decahydrate 99% (0.1 % final concentration) and tween 20
214 (0.5% final concentration). Samples were then shaken for 30 min (150 rpm) at dark and
215 room temperature conditions, left 10 min at 4 ºC, and sonicated with ice during two
216 cycles of 1 min and gently shaken. Samples were left for 5 min for sedimentation of
217 larger particles and supernatant (1 ml) was placed in an Eppendorf. Nycodenz (1 ml)
218 was added to the bottom of the Eppendorf and samples were centrifuged (14 000 rpm)
219 for 90 min at 4 ºC. Purified extract (400 µl) was stained with Syto13 (4 µl, Fisher, 5 µM
220 solution) and incubated in the dark for 30 min. Stained samples were counted using
221 flow cytometry. To normalize fluorescence data, a bead solution (10 µl of 10^6 beads·ml$^-$

222 ^{1}, Fisher 1.0 µm) was added to the samples in a known concentration. Results are
223 reported as bacterial cells·10^6·g DW^{-1}.

224 Bacterial viability was determined also by flow cytometry (FACSCalibur, Becton
225 Dickinson). Pyrophosphate (5 ml, 50 mM - Quéric et al. (2004) -) was added to each
226 fresh sand sample and incubated for 15 min at room temperature and softly shaken, and
227 then sonicated for 1 min with ice to avoid cell disruption (Amalfitano and Fazi, 2008).
228 A subsample of the extract (1 ml) was diluted with 0.2 µm filtered inlet water (1:10).
229 Diluted extract (400 µl) was stained with propidium iodide and Syto 9 (3 µl, BacLight
230 Bacterial Viability Kit) (Falcioni et al. 2006). Samples were incubated in the dark for 15
231 min. According to Falcioni et al. (2006), to normalize fluorescent data a bead solution
232 (10 µl of 10^6 beads · ml^{-1}, Fisher 1.0 µm) was added to the samples in a known
233 concentration. Bacteria Live/Dead ratio was then calculated.

234 Density of live bacteria for each sample was calculated dividing the live/dead ratio by
235 the live/dead ratio plus 1 and then multiplying by the bacterial density. Results are given
236 as number of live cells·10^6·g DW^{-1}. Density of dead bacteria was calculated dividing 1
237 by the live/dead ratio plus 1 and then multiplying by the density of bacteria. Results are
238 given as number of dead cells·10^6·g DW^{-1}. Data from live and dead bacteria densities
239 were transformed to carbon units (µg C·g DW^{-1}) by using the conversion factor of 1.7
240 gC (x 10^{-13}) /cell (Bratbak, 1985).

241 **2.6. Biofilm activity: Extracellular enzyme activities**

242 Extracellular enzyme activities (EEAs) β-glucosidase (EC 3.2.1.21), phosphatase (EC
243 3.1.3.1) and leucine-aminopeptidase (EC 3.4.11.1) were measured using fluorescent-
244 linked artificial substrates (Methylumbelliferyl (MUF)-β-D-glucopyranoside, MUF-β-
245 D-xyloside, MUF-phosphate, and L-leucine-7-amido-4-methylcoumarin hydrochloride
246 (Leu-AMC, Sigma-Aldrich). All enzyme activities were measured under saturating

247 conditions (0.3 mM). Sand samples (1 cm^3) were placed in falcon tubes with filtered
248 (nylon filters 0.2 µm, Whatmann) synthetic water (4 ml) and artificial substrate (120
249 µl). A blank for each artificial substrate was prepared with autoclaved Milli-Q water to
250 determine the abiotic hydrolysis of the substrate itself. Samples and blanks were
251 incubated for 1 hour in the dark with agitation; then, glycine buffer (4 ml, pH 10.4) was
252 added to each falcon tube to stop the reaction and maximize MUF and AMC
253 fluorescence. Samples were centrifuged (2000 g) for 2 minutes, and the supernatant
254 (350 µl) of each sample was placed into a 96 wells black plate (Greiner bio-one) for
255 measuring the fluorescence (excitation/emission wavelengths of 365/455 –MUF- and
256 364/445 –AMC-) in a fluorimeter plate reader (Tecan, infinite M200 Pro). To link
257 fluorescence data and extracellular enzyme activities concentration, MUF and AMC
258 standards were prepared. Results are expressed as nmol $MUF \cdot gDW^{-1} \cdot h^{-1}$ and nmol
259 $AMC \cdot gDW^{-1} \cdot h^{-1}$.

260 **2.7. Statistical analysis**

261 Biomass and EEAs differences in depth were analyzed with ANOVA (factor: depth)
262 and further Tukey post-hoc analysis. ANOVA (factor: system) was also applied at each
263 depth to determine significant differences of biofilm parameters depending on GSDs.
264 Dynamics of biomass data measured at each depth and system were fitted with LOcally
265 Estimated Scatterplot Smoothing –LOESS curve fitting- (*Loess* stats package), (n = 27
266 for data from the top and mid layers, n = 24 for the bottom layer). Regular sequences of
267 time were generated for further interpolation at each LOESS curve to estimate
268 continuous data over time (frequency = 7 days). With the regular sequences created
269 with the LOESS curve fitting, comparison of biomass dynamics between systems and
270 among depths were performed by using the cross-correlation function estimation (stats
271 package *ccf*). Temporal K/K_0 values were also LOESS curve fitted to visualize system

272 dynamics (n = 75) at each depth layer. ANOVA analysis was performed for hydraulic
273 conductivity reduction data (K/K_0) at each depth layer separately (factor: system) to
274 detect significant differences between GSDs. Multivariate analysis with biofilm and
275 K/K_0 data was performed through principal component analysis (PCA) (*ggplot* in
276 ggplot2 package). Previously, data for the multivariate analysis was standardized
277 separately for each depth (subtracting the mean and dividing by the standard deviation).
278 Carbon contribution of each biofilm-component to the overall C content in sands was
279 plotted in a percentage stacked bar chart (*ggplot* in ggplot2 package). All statistical
280 analyses and plots have been performed using R software (version 3.1.1).

281 ## 3. Results

282 Biofilm structural components (algae, EPS, live and dead bacteria) and biofilm EEAs
283 (β-glucosidase, phosphatase and leucine-aminopeptidase) displayed a vertical
284 decreasing gradient, with the highest values measured in the top layer (values in the mid
285 and bottom layers were at least one order of magnitude smaller than those measured at
286 the top one -Fig. 2, Fig. 3-). In the top layer, no differences in biomass were observed
287 between systems except for higher density of live bacteria in the CF system. In the mid
288 layer, algae and bacterial density (both live and dead) were higher in CF than in F. In
289 the bottom layer, live and dead bacteria densities were higher in CF system than in F.
290 Complementarily, Margalef pigment index showed an increasing trend in depth in both
291 systems (Table S2).

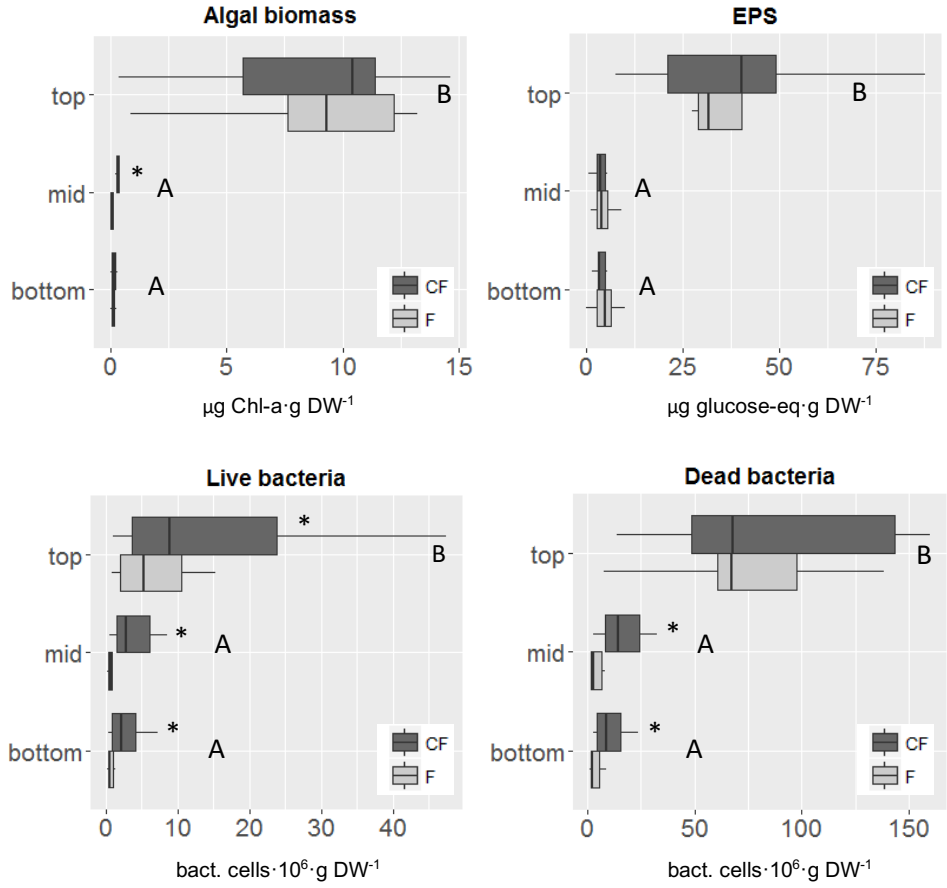

Figure 2 Biofilm structural parameters in depth (top and mid depths based on n = 9 data; bottom n = 8). Capital letters (A, B) indicate statistically significant differences in depth (ANOVA, factor: depth, $p < 0.05$), asterisks indicate statistically significant higher biomass values in CF than in F (ANOVA, factor: system, $p < 0.05$).

With regards to EEAs in the top layer, both systems showed similar activity (per units of dry weight and per live bacteria density) (Fig. 3). In the mid layer, CF showed higher β-glucosidase activity (per units of dry weight and per live bacteria density), leucine-aminopeptidase activity (per units of dry weight and per live bacteria density) and phosphatase activity (per units of dry weight) than F. The CF system also showed higher leucine-aminopeptidase activity in the bottom layer (per units of dry weight and per live bacteria density) compared to F.

Extracellular enzyme activities

EEAs per dry weight **EEAs per live bacteria**

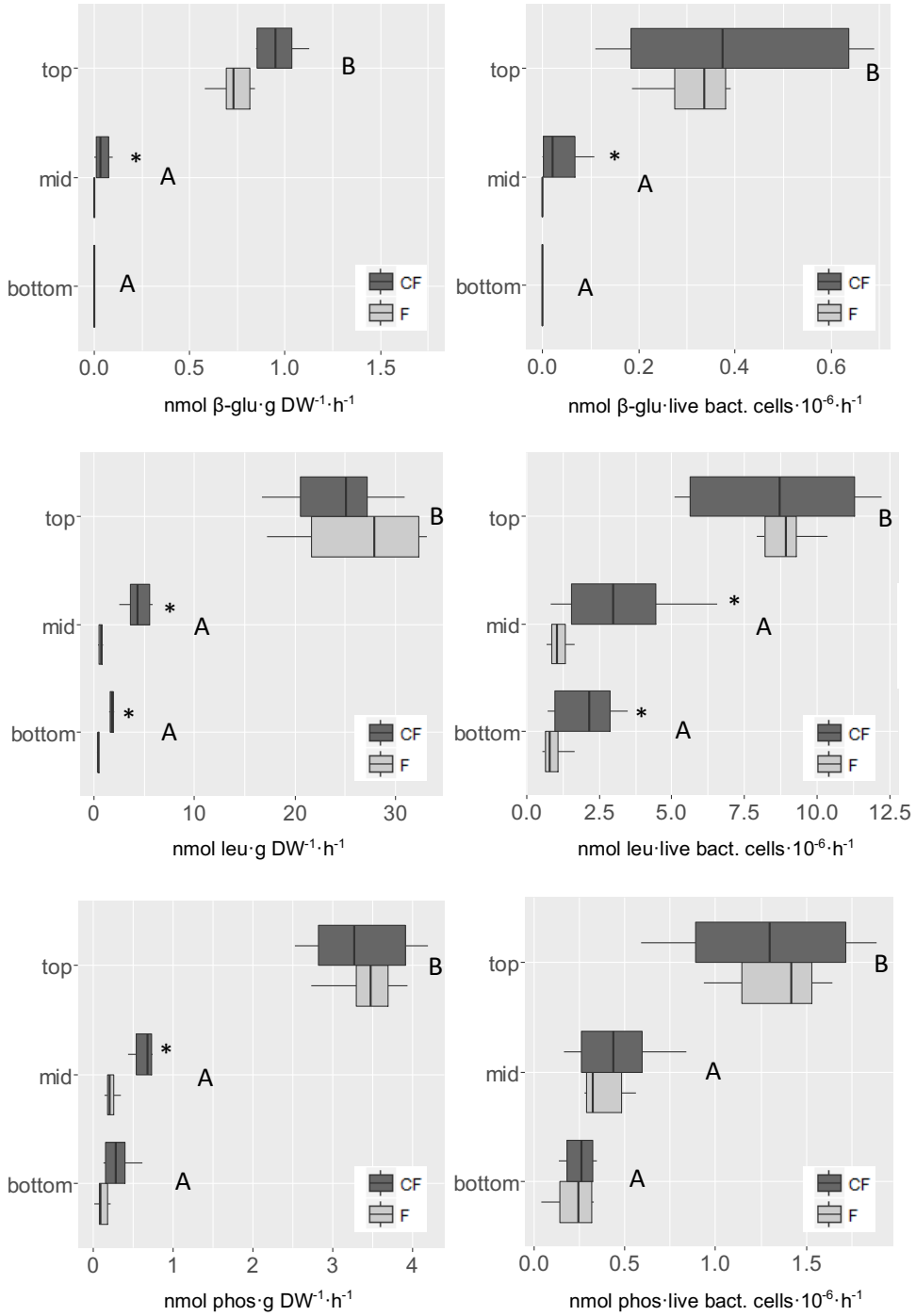

Figure 3 Extracellular enzyme activities in depth (data from days 47 and 105). Capital letters (A, B) indicate statistically significant differences in depth (ANOVA, factor: depth, $p < 0.05$). Asterisks indicate statistically significant higher EEA values in CF than in F (ANOVA, factor: system, $p < 0.05$). β-glu: β-glucosidase; leu: leucine-aminopeptidase; phos: phosphatase.

Biofilm colonization of algae, EPS, live bacteria and dead bacteria in the top layer showed similar dynamics in both systems (all correlations were significant, $R^2 > 0.5$, Fig. 4). Algal biomass and EPS concentrations showed an increasing trend until day 40

317 when they almost stabilized; contrarily, bacterial density (both live and dead) reached
318 peak values at around day 30, followed by a decrease. However, algal dynamics showed
319 a slight delay in the CF system compared to F (the exact value cannot be given due to
320 the sampling intervals, but as an interval, here 0-7 days). Furthermore, algae and EPS
321 showed an increasing trend around the end of the experiment in CF, indicating that
322 stationarity might not had been achieved.

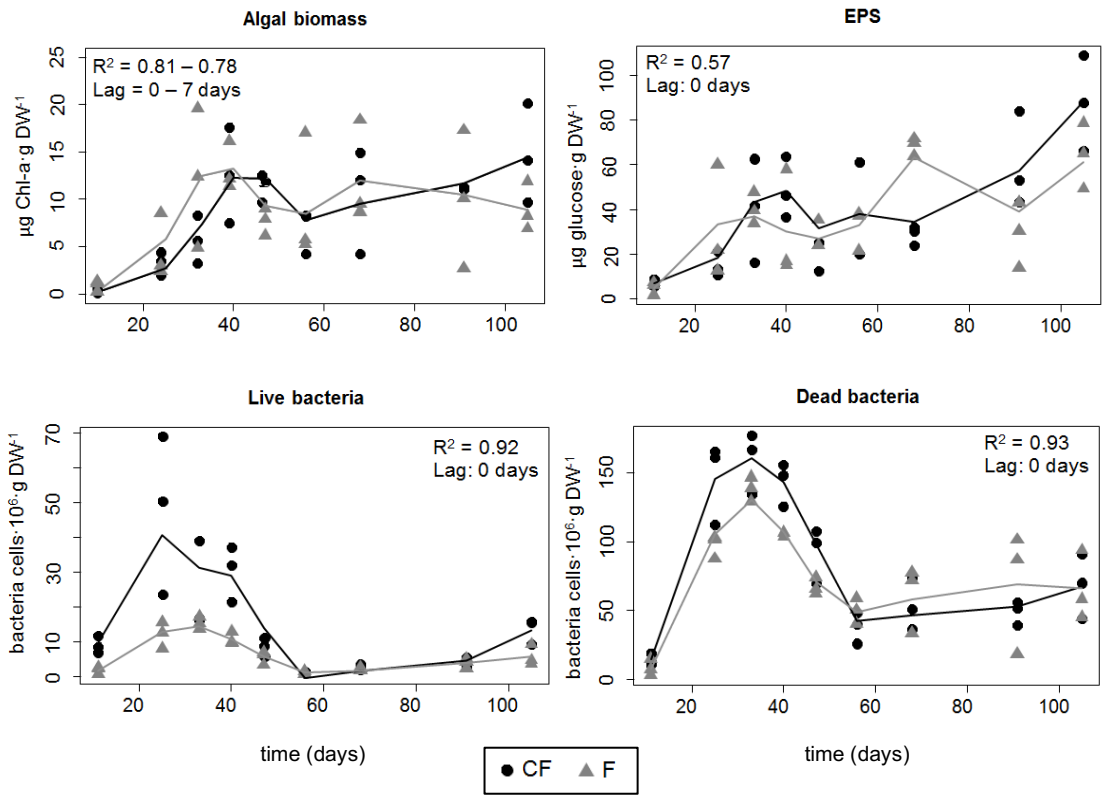

323

324

325

326 **Figure 4** Colonization dynamics of algae, EPS, live bacteria and dead bacteria densities
327 measured in the top layer at each system. Solid lines show LOESS curve fitting (n = 27) for
328 each system. R^2 values indicate temporal dynamics linear correlation between systems. R^2
329 critical = 0.5; values below indicate no significant correlation in biofilm dynamics between
330 systems.

331 In depth, biofilm accumulation dynamics (see Fig. S2 and Fig. S3 in the supplementary
332 material) arise from the conjunction of biofilm growing in deep layers and biomass
333 detachment from upper layers, transported downwards, and then reattached to the pore
334 network downwards. Biofilm depth-dynamics were studied by statistical cross-

335 correlations among depths (Table 1). Algae, live bacteria and dead bacteria present at 20
336 cm depth showed positive correlation with the values measured in the top layer in both
337 systems (Table 1). Bacterial density correlations showed no lag (no delay) but algal
338 biomass values at 20 cm depth displayed a delay compared to those in the top layer,
339 suggesting biomass detachment from the top layer and further downward transport of
340 the autotrophic biomass in both systems. Regarding EPS, no correlations between
341 surface and 20 cm depth were found in the case of the CF system, but in the F system a
342 0-7 day lag-phase was found, suggesting EPS detachment from the top layer and
343 accumulation in depth in the F system, but not in the CF one.

344 Focusing on correlations from the different variables measured at depths 20 and 40 cm,
345 the F system showed a strong correlation in depth-dynamics for all the parameters
346 studied (algae, EPS, live bacteria and dead bacteria) (Table 1), indicating similar
347 accumulation dynamics in depth. However, the CF system showed positive correlation
348 on live and dead bacteria dynamics measured at 20 and 40 cm depth –with a lag phase
349 around 7 days at 40 cm depth -, but no depth-correlation was reported for algae or EPS.

350

Table 1 Cross-correlations of biofilm parameters among depths[1].

		CF	F
Top →Mid n = 14 critical $R^2 = 0.5$	Algae	**$R^2 = 0.50$** Lag: 7 days	**$R^2 = 0.73$** Lag: 7 days
	EPS	$R^2 < 0.5$ Lag: -	**$R^2 = 0.61$** Lag: 0-7 days
	Live Bacteria	**$R^2 = 0.87$** Lag: 0 days	**$R^2 = 0.92$** Lag: 0 days
	Dead Bacteria	**$R^2 = 0.85$** Lag: 0 days	**$R^2 = 0.83$** Lag: 0 days
Mid →Bottom n = 12 critical $R^2 = 0.55$	Algae	$R^2 < 0.55$ Lag: -	**$R^2 = 0.72$** Lag: 0 days
	EPS	$R^2 < 0.55$ Lag: -	**$R^2 = 0.63$** Lag: 0 days
	Live Bacteria	**$R^2 = 0.75$** Lag: 7 days	**$R^2 = 0.95$** Lag: 0 days
	Dead Bacteria	**$R^2 = 0.77$** Lag: 7 days	**$R^2 = 0.94$** Lag: 0 days

[1]Values in bold indicate significant correlation among depths at each system for each parameter. Lag phase corresponds to the day at which the maximum correlation is achieved.

Hydraulic conductivity showed high variability over time resulting in K/K_0 oscillations (Fig. 5). The highest effect of bioclogging upon hydraulic conductivity reduction was found in the top 5 cm of infiltration (Fig. 5a), where K/K_0 measurements ranged from 0.43 – 0.76 (CF) and from 0.32 – 0.69 (F), indicating a maximum hydraulic conductivity decrease of 57 % in CF and 68 % in F. From 5 to 20 cm depth (Fig. 5b), K/K_0 ranged from 0.46-0.96 in CF and from 0.77-1.17 in F (maximum K reduction of 54 % in CF and 23 % in F). Last, from 20 to 40 cm depth (Fig. 5c) K/K_0 values in CF ranged from 0.89 – 1.04 and in F from 0.69 – 0.93 (maximum K reductions of 11 % and 31 % in CF and F, respectively). When the system was analyzed as a whole (Fig. 5d), the F system showed a maximum K reduction of 47 % and CF of 29 %. ANOVA results showed that the F system developed higher bioclogging than CF in the upper and bottom layers and overall, while the opposite happened in the middle layer.

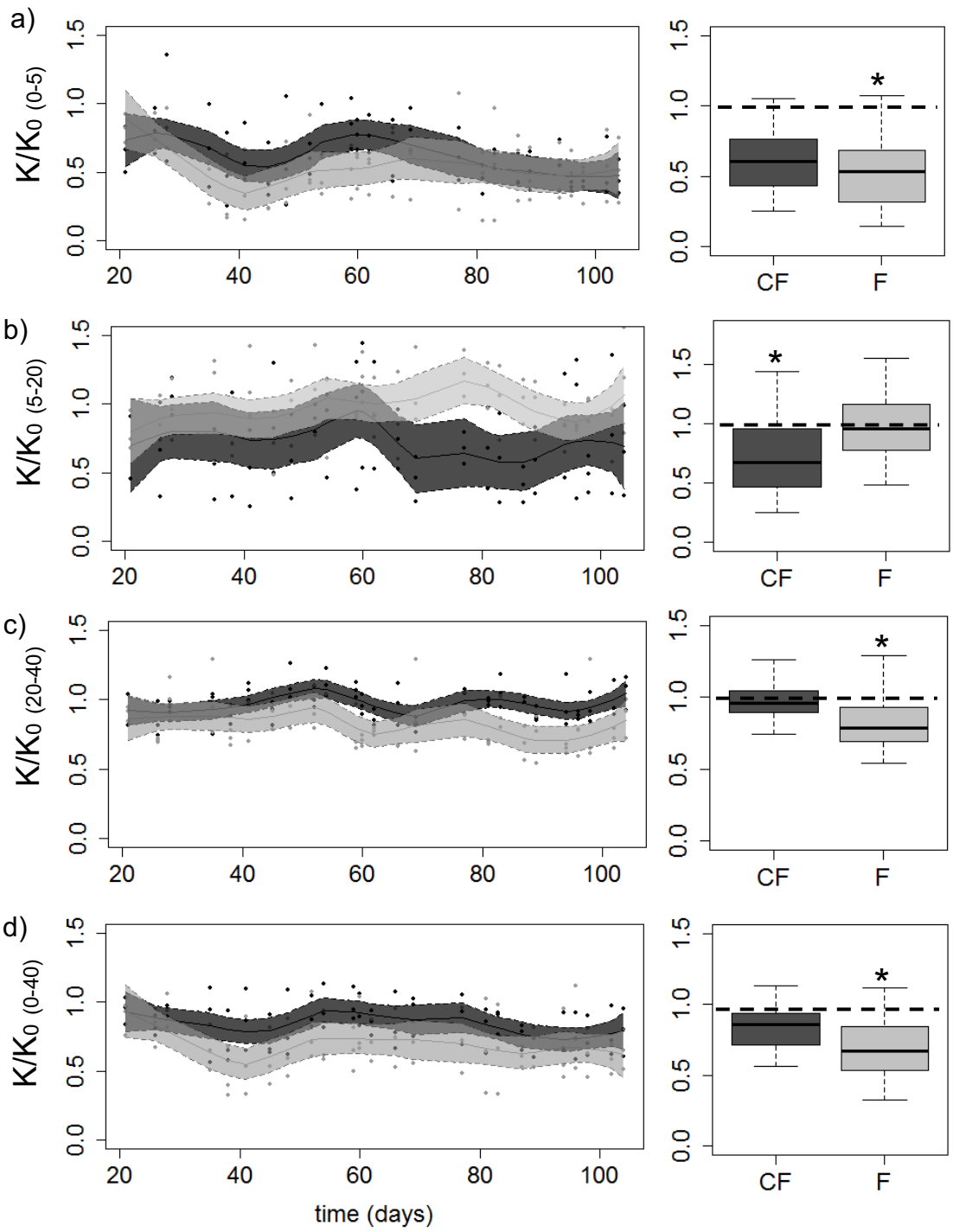

Figure 5 Left: Hydraulic conductivity variations (K/K_0) over time measured at different depths (a: 0 - 5 cm, b: 5 - 20 cm, c: 20 - 40 cm and d: 0 - 40 cm) fitted with LOESS curve fitting (n = 75 for each curve) and polygon bounds indicating 95% of data lying assuming a normal distribution for each curve. Dark lines: CF; light lines: F. Right: boxplots of measured data (the dashed lines indicate $K=K_0$). Asterisks indicate the system with higher bioclogging at each layer (ANOVA, factor: system, $p < 0.05$).

Figure 6 displays the results of the PCA analyses for each depth including hydraulic conductivity variations and biofilm representative parameters. In the top layer (upper 5 cm), both CF and F systems showed similar responses of biological and hydraulic

parameters (Fig. 6a): variations in K closely related to algal biomass and EPS content while densities of live and dead bacteria were uncorrelated to K variations or to EPS and algae concentrations. Clear differences were found between systems at 20 cm depth (Fig. 6b). From 5 to 20 cm depth, lower values of K/K_0 in the CF system correlated to higher bacterial and algal biomass at 20 cm depth compared to the F system. In the bottom layer, lower K/K_0 values in F were strongly correlated to EPS concentration in depth (Fig. 6c).

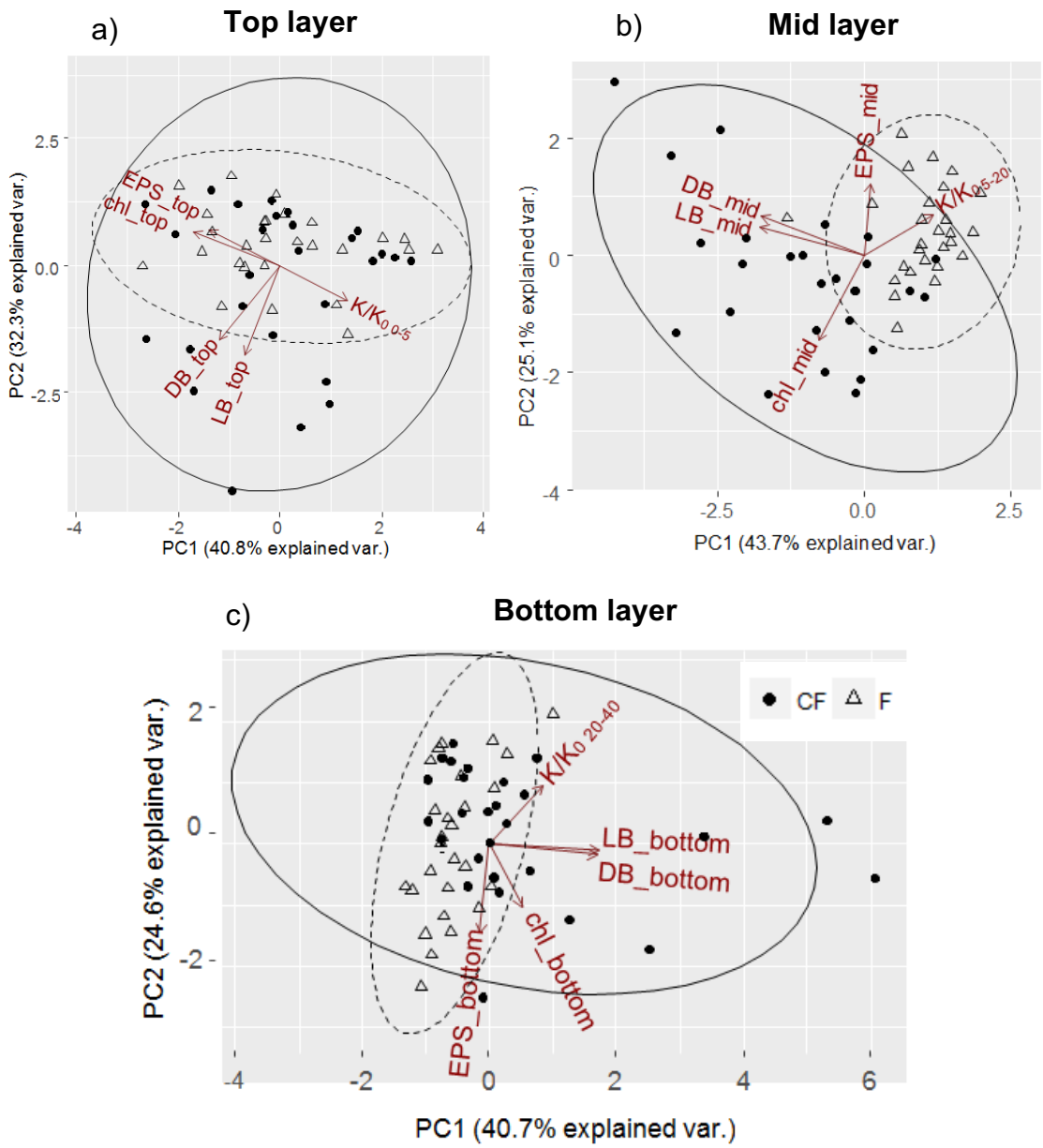

Figure 6 Plot of the PCA analysis including hydraulic and biofilm structural parameters at different depths (top layer: 0 - 5 cm, mid: 5 - 20 cm, bottom: 20 - 40 cm). LB: Live bacteria; DB: Dead bacteria; chl: chlorophyll-a as a proxy of algal biomass.

390 Contribution of each biofilm structural component to the overall biofilm organic carbon
391 showed that algae contributed the most to the overall organic carbon measured in sands,
392 decreasing this contribution from the top (≈ 90% of total carbon) to the mid and bottom
393 layers where it still represented 50% of the total organic carbon content. The
394 contribution of EPS and dead and live bacteria increased from top to mid and bottom
395 layers in both systems. In depth, EPS contributed ≈ 30%, dead bacteria ≈ 25% and live
396 bacteria ≈ 10% of the overall biofilm organic carbon, at most (Fig. S4).

397 ## 4. Discussion

398 ### *4.1 Biofilm colonization in different grain-sized porous media*

399 Decreasing trends of biomass and biofilm activity in depth have been widely reported in
400 porous media (Yan et al. 2017; Freixa et al. 2016; Mermillod-Blondin et al. 2005),
401 mainly attributed to a decrease in the availability of nutrients in depth, thus constraining
402 biomass growth (Battin and Sengschmitt, 1999). Disregarding temporal fluctuations -
403 explained by biofilm attachment, adhesion, proliferation, maturation and detachment
404 phases (Lappin-Scott and Costerton, 1989)-, both fine (0.075 - 0.25 mm) and coarse
405 (0.9 – 1.2 mm) sands showed similar ability for biofilm colonization since both systems
406 achieved similar overall biomass densities in the top layer, excepting greater live
407 bacteria accumulating in CF. Although we did not measure bacterial density in the inlet
408 water, other studies showed that WWTPs outflow water carry bacterial densities of
409 around 10^8 cells·ml^{-1} (e.g., Vivas et al. 2017); this implies that the larger hydraulic
410 conductivity (and consequently higher bacterial loads) in the bilayer CF system with
411 respect to the monolayer F one would result in the largest bacterial density in the former
412 system.

413 However, biofilm colonization dynamics in the top layer were distinct in both systems.
414 Biofilm colonization occurred earlier in the monolayer F system than in the CF one,

possibly driven by the combination of low fluxes and high surface area in the former (Donlan, 2002) which could have favored biomass attachment and accumulation (Fang et al. 2017).

Biofilm growth asymptotically approaches steady state as the result of the balance between biomass decay/detachment and growth (Bottero et al. 2013). Linked to this, the increasing trend in algae, EPS and live bacteria densities at the end of the experiment in the bilayer CF system suggests a transient effect due to still existing available space for biomass growth mostly in the coarse sand. On the contrary, biofilm in the top layer of the monolayer F system could have reached a maturity state resulting in equilibrium between the biomass detachment and accrual terms.

4.2 Grain-size distribution of the porous media modulating deep bioclogging: biofilm attachment, detachment and vertical transport

Differences observed on biomass dynamics in depth between systems could be due to biomass depth-accumulation being a conjunction between solute availability in depth, flux rates, and detachment/attachment dynamics, all influenced by GSDs. Linked to this, EPS accumulation in depth is driven both by biomass downward transport and by EPS bacterial production. Interestingly, EPS detachment from the top layer and further transport seems to be the main EPS accumulation pathway in depth in the monolayer F system. Contrarily, no EPS correlation in depth in the bilayer CF system as well as higher density of live bacteria suggested EPS production by bacteria to be the main pathway for EPS accumulation in depth in the bilayer system.

High flow velocities result in thin but strong biofilm matrices, while under low fluxes, thicker and less cohesive (more detachable) biofilms are observed (Gerbersdorf and Wieprecht 2015, Laspidou and Rittmann 2002, Graba et al. 2013). Thus, under high flow, and correspondingly high shear forces (as expected in the bilayer CF system), a

440 denser, cohesive, and more stable biofilm is likely to be produced because of strong
441 adherence to the EPS matrix in comparison to biofilms subjected to low shear forces
442 (Oyebamiji et al. 2018), such as the monolayer F system. Furthermore, biofilm reaching
443 steady state in the top layer (F system) could have enhanced biofilm detachment and
444 transport in depth, following Liu and Tay (2002), who observed that mature biofilms
445 were strongly affected by hydrodynamic shear stresses. This reinforces the idea that
446 combined hydraulic and biofilm dynamics, both modulated by GSD, may strongly
447 influence biofilm detachment in porous media.

448 It is widely accepted that advection is the main mechanism for transport of dissolved
449 and particulate matter (as well as detached biofilm) through the interstitial space (e.g.,
450 Zhong et al. 2017; Huettel et al. 1998), so that the effect of diffusion can be neglected.
451 Nonetheless, heterogeneity of the pore structure results in preferential flows during
452 infiltration (e.g., Rubol et al., 2014) being the source of hydrodynamic dispersion and
453 driving mixing (Rodriguez-Escales et al., 2017). Heterogeneity is enhanced at interfaces
454 between materials (e.g., coarse and fine sands), where a large distribution of local
455 velocities spanning several orders of magnitude can be found. Consequently dispersion,
456 forced by the presence of a strong variation in local velocities, could have produced the
457 conditions to depth-trapping algal and bacterial biomass hindering advective biomass
458 transport from the interface downwards in the bilayer CF system.

459 All these biofilm dynamics showed great implications on the occurrence of bioclogging.
460 Specifically, the monolayer F system showed higher degree of bioclogging in the top
461 layer and in the bottom one. This could be due to the monolayer F system developing
462 similar density of biomass in the top layer (specifically EPS and algae which are the
463 main contributors of surface bioclogging) but lower pore sizes (also slightly lower
464 porosity) than the bilayer CF system, thus promoting surface bioclogging. Yet, the

465 expected biofilm is non-cohesive, and large amounts are detached and transported
466 downward, allowing for additional pore space to grow additional biofilm on top while
467 also detached biomass having the potential to accumulate in depth, causing deep
468 bioclogging. According to Watnick and Kolter (2000), detached biomass cause the
469 spreading of biofilms along the advective path, as they are the primary mechanism for
470 translocation from one surface to another.

471 Our results indicate that biofilm biomass can reach depths of at least 40 cm in both fine
472 (0.075 – 0.25 mm) and coarse (0.9 – 1.2 mm) sands. Specifically, EPS concentrations at
473 40 cm depth (accounting only for 15-20 % of the overall carbon biomass in the biofilm)
474 seem to be the main cause of deep bioclogging in the monolayer F system. Even though
475 EPS densities in the bottom layer were similar in both systems, EPS quality could be
476 different between systems thus showing a different effect on bioclogging. Note that
477 although algal biomass at 40 cm depth represented the main structural component of
478 biofilms in terms of C, it does not show direct implications on deep clogging possibly
479 due to its degraded state in the bottom layers. In depth, the presence of degraded algae is
480 expected due to the lack of incident light, thus limiting its growth, and validated by the
481 increasing values of the Margalef pigment index with depth indicating an increase in
482 chlorophyll degradation products.

483 ### *4.3 A bilayer coarse-fine distribution: minimizing bioclogging in infiltration systems*

484 Maybe less intuitive is the potential of the interface coarse-fine to minimize the
485 occurrence of deep clogging in infiltration systems. Even though the interface becomes
486 the location for biomass accumulation, our results suggest that it also results in a hot-
487 spot of microbial activity (as highlighted by Perujo et al. 2017) which causes the
488 presence of high EEA values in depth and high live bacteria densities, thus helping
489 maintaining the hydraulic conductivity values of the porous media with time.

On the contrary, the monolayer fine system exhibited higher bioclogging in all layers; so, as a whole, it exhibited large overall (non-localized) bioclogging due possibly to the combination of strong biomass detaching and recolonization in the top layer. Furthermore, in the monolayer system, low EEA values in depth, low bacterial viability and low availability of solutes could contribute to high biomass and organic matter accumulation in depth in the long term.

4.4 Relevance of the Findings and Limitations of the Study

Results from the present study state that bioclogging occurrence in infiltration systems can be reduced by controlling the characteristics of filter media such as GSD as well as by understanding biofilm dynamics in surface and in depth. Altogether, this study may help improving the design and maximizing the performance of infiltration systems used as tertiary water treatment systems.

Successful performance of infiltration systems requires maintaining relatively high hydraulic conductivity values of the system as a whole to convey water efficiently from the surface downwards during periods of system operation (Racz et al. 2012); thus it is important to reduce the land use necessary for their application (Bouwer, 2002), the maintenance operations, and the overall cost. By adding a layer of coarse sand on top in systems where the natural material is fine sands: (1) we are able to infiltrate higher volume of water per surface area unit than in a monolayer system (only fine material); (2) surface and deep bioclogging are minimized, increasing the longevity of the infiltration system and keeping the high infiltrating volumes for longer times, and (3) water treatment efficiency is maintained, as previously reported in Perujo et al. (2018).

This study could also benefit further understanding and provide useful modelling tools to capture the effects of the biofilm growing stage on biofilm dynamics such as attachment/detachment influenced by hydrodynamics and GSD of the porous media and

515 their influence not only on surface but also on deep bioclogging. Agreeing with Smith et
516 al. (2018), the lack of data and understanding of microbial processes has challenged so
517 far the incorporation of microbial ecology into bioclogging models.

518 We also observed that biofilm-component dynamics are not the same for bacteria, EPS
519 and algae, so differentiation between these parameters should be done in future studies
520 addressing bioclogging. Also, in the future it would be interesting to study the role of
521 EPS fractions on deep bioclogging linked to EEAs. Accordingly, EPS can be classified
522 in two main fractions: colloidal EPS that is soluble in water and secreted in the vicinity
523 of cells, and bound EPSs that is tightly attached to the cell walls (Chen et al. 2017).
524 Different EPS fractions may have distinct impacts on driving hydrological changes
525 within the porous media.

526 ## Conclusions

527 From this experimental study we could state that biofilm structural parameters showed
528 different dynamics and implications on bioclogging in infiltration systems. In particular,
529 grain-size distribution along the vertical has a strong influence in biomass attachment.
530 In fine sands, higher availability of surface area as well as lower fluxes could favor the
531 initial biofilm formation phase (attachment) as compared with coarse sands. This
532 translates to an early biofilm formation in the monolayer fine system considered in the
533 field experiment analyzed in this work, which resulted in an early surface bioclogging
534 (also favored by the smaller pore sizes, easily colonizable). At the same time, this early
535 biofilm formation resulted in an early maturation stage of the biofilm, which promoted
536 biomass detachment from upper layers and further recolonization of the topsoil by new
537 biomass. Further, the presence of a homogeneous grain size enhanced the transport of
538 biomass in depth modulating not only the occurrence of surface bioclogging but also
539 deep bioclogging.

Contrarily, in the bilayer coarse-fine system we observed an active biofilm with high activity per surface unit (which includes organic matter degradation and thus helps to control bioclogging). The interface in the bilayer system acted as a biomass filter with a hot-spot of microbial activity which minimized deep bioclogging. This is due to this interface trapped biomass in a middle-depth where availability of solutes is higher promoting microbial activity in the interface with additional implications in deeper layers. As a whole, a bilayer system with an upper layer of coarse sands (around 1 mm) showed similar biofilm colonization than fine sands (0.075 – 0.250 mm) and higher overall biofilm activity minimizing bioclogging, and therefore, having the potential to increase the longevity and efficiency of infiltration systems.

Acknowledgements

We acknowledge support from TRARGISA – Depuradora de Girona, especially to Cristina and Lluís. This work was supported by the Spanish Ministry of Economy and Competitiveness (GL2014-58760-C3-2-R and project ACWAPUR - PCIN-2015–239), the ERA-NET Cofund Waterworks 2014, the Department of Universitats, Recerca i Societat de la Informació de la Generalitat de Catalunya (ref 2017 SGR 548), and the European Social Fund.

Supporting Information. Scheme and photograph of the experimental design used for piezometric head measurements; accumulation dynamics of biofilm-structural components in the mid and bottom layers; percentage of carbon content of each of the biofilm-structural components from the total biofilm carbon; values of hydraulic conductivity measured at day 19 at each depth layer; Margalef pigment index calculated for each system and depth.

References

AEMET - State Agency of Meteorology Website. Ministry of the Environment and Rural and Marine Affairs, Spanish Government. (AEMET - Agencia Estatal de meteorología. Ministerio de Medio Ambiente y Medio Rural y Marino, Gobierno de España). http://www.aemet.es/es/serviciosclimaticos/vigilancia_clima/analisis_estacional (accessed Feb 12, 2017).

Amalfitano, S.; Fazi, S. Recovery and quantification of bacterial cells associated with streambed sediments. *J. Microbiol. Methods* **2008**, 75, 237–243; DOI 10.1016/j.mimet.2008.06.004

Amalfitano, S.; Fazi, S.; Puddu, A. Flow cytometric analysis of benthic prokaryotes attached to sediment particles. *J. Microbiol. Methods* **2009**, 79, 246–249; DOI 10.1016/j.mimet.2009.09.005

Barai, P.; Kumar, A.; Mukherjee, P. P. Modeling of mesoscale variability in biofilm shear behavior. *PLoS One* **2016**, 11, 1–16; DOI 10.1371/journal.pone.0165593

Bardin, J. P.; Barraud, S.; Alfakih, E.; Dechesne, M. Performance assessment of stormwater infiltration strategies: A multi-indicator approach. In *Global Solutions for Urban Drainage*; Strecker, E. W., Huber, W. C., Eds.; American Society of Civil Engineers (ASCE): Reston 2002; pp 1-14.

Battin, T. J.; Sengschmitt, D. Linking sediment biofilms, hydrodynamics, and river bed clogging: evidence from a large river. *Microbial Ecology* **1999**, 37(3), 185-196.

Battin, T. J. Hydrodynamics is a major determinant of streambed biofilm activity: From the sediment to the reach scale. *Limnol. Oceanogr*. **2000**, 45, 1308–1319.

Battin, T. J.; Besemer, K.; Bengtsson, M. M.; Romani, A. M.; Packmann, A. I. The ecology and biogeochemistry of stream biofilms. *Nature Reviews Microbiology* **2016**, 14(4), 251.

Baveye, P.; Vandevivere, P.; Hoyle, B.L.; DeLeo, P.C.; de Lozada, D.S. Environmental impact and mechanisms of the biological clogging of saturated soils and aquifer materials. *Crit. Rev. Environ. Sci. Technol*. **1998**, 28, 123-191; DOI 10.1080/10643389891254197.

Bouwer, H.; Rice, R. C. Effect of water depth in groundwater recharge basins on

infiltration. *Journal of Irrigation and Drainage Engineering* **1989**, 115(4), 556-567.

Bouwer, H. Artificial recharge of groundwater: hydrogeology and engineering. *Hydrogeology Journal* **2002**, 10(1), 121-142.

Bottero, S., Storck, T., Heimovaara, T. J., van Loosdrecht, M. C., Enzien, M. V.; Picioreanu, C. Biofilm development and the dynamics of preferential flow paths in porous media. *Biofouling* **2013**, 29(9), 1069-1086.

Brangarí, A. C., Fernàndez-Garcia, D., Sanchez-Vila, X., Manzoni, S. Ecological and soil hydraulic implications of microbial responses to stress–A modeling analysis. *Advances in water resources* **2018**, 116, 178-194.

Bratbak, G. Bacterial biovolume and biomass estimations. *Applied and Environmental Microbiology* **1985**, 49(6), 1488-1493.

Campos, L. C.; Su, M. F. J.; Graham, N. J. D.; Smith, S. R. Biomass development in slow sand filters. *Water research* **2002**, 36(18), 4543-4551.

Camprovin, P.; Hernández, M.; Fernández, S.; Martín-Alonso, J.; Galofré, B.; Mesa, J. Evaluation of clogging during sand-filtered surface water injection for aquifer storage and recovery (ASR): Pilot experiment in the llobregat delta (Barcelona, Spain). *Water* **2017**, 9(4), 263; DOI 10.3390/w9040263

Chen, X. D.; Zhang, C. K.; Zhou, Z.; Gong, Z.; Zhou, J. J.; Tao, J. F.; Paterson, D.M.; Feng, Q. (2017). Stabilizing effects of bacterial biofilms: EPS penetration and redistribution of bed stability down the sediment profile. *Journal of Geophysical Research: Biogeosciences* **2017**, 122(12), 3113-3125.

Dechesne, M.; Barraud, S.; Bardin, J. P. Indicators for hydraulic and pollution retention assessment of stormwater infiltration basins. *J. Environ. Manage*. **2004**, 71, 371–380; DOI 10.1016/j.jenvman.2004.04.005

de Matos, M. P.; von Sperling, M.; de Matos, A. T. Clogging in horizontal subsurface flow constructed wetlands: influencing factors, research methods and remediation techniques. *Reviews in Environmental Science and Bio/Technology* **2018**, 1-21.

Dillon, P.; Page, D.; Vanderzalm, J.; Pavelic, P.; Toze, S.; Bekele, E.; Sidhu, J.;

622 Prommer, H.; Higginson, S.; Regel, R.; Rinck-Pfeiffer, S.; Purdie, M.; Pitman, C.;
623 Wintgens, T. A critical evaluation of combined engineered and aquifer treatment
624 systems in water recycling. *Water Sci. Technol.* **2008**, 57, 753–762; DOI
625 10.2166/wst.2008.168

626 Ding, Y., Lyu, T., Bai, S., Li, Z., Ding, H., You, S., Xie, Q. Effect of multilayer
627 substrate configuration in horizontal subsurface flow constructed wetlands:
628 assessment of treatment performance, biofilm development, and solids
629 accumulation. *Environmental Science and Pollution Research* **2018**, 25(2), 1883-
630 1891.

631 Donlan, R. M. Biofilms: microbial life on surfaces. *Emerging infectious diseases* **2002**,
632 *8*(9), 881.

633 Duan, Y. L.; Ji, X. C.; Yu, Y. Y.; Li, Y. H. Clogging of the subsurface infiltration
634 system. In: Architectural, Energy and Information Engineering: Proceedings of the
635 2015 International Conference on Architectural, Energy and Information
636 Engineering (AEIE 2015), Xiamen, China, May 19-20, 2015; Sung, W. P., Chen,
637 R., Eds.; CRC Press: New York 2015; pp 193.

638 Dubois, M.; Gilles, K. A.; Hamilton, J. K.; Rebers, P. T.; Smith, F. Colorimetric method
639 for determination of sugars and related substances. *Anal. Chem.* **1956**, 28, 350–
640 356; DOI 10.1021/ac60111a017

641 Dupin, H. J.; Kitanidis, P. K.; Mccarty, P. L. Pore-scale modeling of biological clogging
642 due to aggregate expansion: A material mechanics approach. *Water Resour. Res.*
643 **2001**, 37, 2965–2979.

644 Falcioni, T.; Manti, A.; Boi, P.; Canonico, B.; Balsamo, M.; Papa, S. Comparison of
645 Disruption Procedures for Enumeration of Activated Sludge Floc Bacteria by Flow
646 Cytometry. *Cytom. Part B Clin. Cytom.* **2006**, 70B, 149–153; DOI
647 10.1002/cyto.b.20097

648 Fang, H.; Chen, Y.; Huang, L.; He, G. Biofilm growth on cohesive sediment deposits:
649 laboratory experiment and model validation. *Hydrobiologia* **2017**, 799(1), 261-
650 274.

651 Farah, T.; Souli, H.; Fleureau, J. M.; Kermouche, G.; Fry, J. J.; Girard, B.; Aelbrecht,

652 D.; Lambert, J.; Harkes, M. Durability of bioclogging treatment of soils. *Journal of*
653 *Geotechnical and Geoenvironmental Engineering* **2016**, 142(9), 04016040.

654 Findlay, S. E. G.; Sinsabaugh, R. L.; Sobczak, W. V.; Hoostal, M. Metabolic and
655 structural response of hyporheic microbial communities to variations in supply of
656 dissolved organic matter. *Limnol. Oceanogr*. **2003**, 48, 1608–1617.

657 Flemming, H.; Wingender, J. The biofilm matrix. *Nature Reviews Microbiology* **2010**,
658 8, 623–633; DOI 10.1038/nrmicro2415

659 Flemming, H. C.; Wingender, J.; Szewzyk, U.; Steinberg, P.; Rice, S. A.; Kjelleberg, S.
660 Biofilms: an emergent form of bacterial life. *Nature Reviews Microbiology* **2016**,
661 14(9), 563-575.

662 Freixa, A.; Rubol, S.; Carles-Brangarí, A.; Fernàndez-Garcia, D.; Butturini, A.;
663 Sanchez-Vila, X.; Romaní, A. The effects of sediment depth and oxygen
664 concentration on the use of organic matter: An experimental study using an
665 infiltration sediment tank. *Sci. Total Environ*. **2016**, 540, 20–31; DOI
666 10.1016/j.scitotenv.2015.04.007

667 Fu, G.; Zhang, J.; Chen, W.; Chen, Z. Medium clogging and the dynamics of organic
668 matter accumulation in constructed wetlands. *Ecological engineering* **2013**, 60,
669 393-398.

670 Gerbersdorf, S. U.; Wieprecht, S. Biostabilization of cohesive sediments: Revisiting the
671 role of abiotic conditions, physiology and diversity of microbes, polymeric
672 secretion, and biofilm architecture. *Geobiology* **2015**, 13, 68–97; DOI
673 10.1111/gbi.12115

674 Gette-Bouvarot, M.; Mermillod-Blondin, F.; Angulo-Jaramillo, R.; Delolme, C.;
675 Lemoine, D.; Lassabatere, L.; Loizeau, S.; Volatier, L. Coupling hydraulic and
676 biological measurements highlights the key influence of algal biofilm on
677 infiltration basin performance. *Ecohydrology* **2014**, 7, 950–964; DOI
678 10.1002/eco.1421

679 Graba, M.; Sauvage, S.; Moulin, F. Y.; Urrea, G.; Sabater, S.; Sanchez-Pérez, J. M.
680 Interaction between local hydrodynamics and algal community in epilithic
681 biofilm. *Water research* **2013**, 47(7), 2153-2163.

682 Gutiérrez, J. P.; van Halem, D.; Uijttewaal, W. S.; del Risco, E.; Rietveld, L. C. Natural
683 recovery of infiltration capacity in simulated bank filtration of highly turbid
684 waters. *Water research* **2018**, 147, 299-310.

685 Hall-Stoodley, L.; Costerton, J. W.; Stoodley, P. Bacterial biofilms: from the natural
686 environment to infectious diseases. *Nature reviews microbiology* **2004**, 2(2), 95.

687 Higashino, M. Quantifying a significance of sediment particle size to hyporheic
688 sedimentary oxygen demand with a permeable stream bed. *Environ. Fluid Mech*.
689 **2013**, 13, 227–241; DOI 10.1007/s10652-012-9262-3

690 Hirst, C. N.; Cyr, H.; Jordan, I. A. Distribution of exopolymeric substances in the
691 littoral sediments of an oligotrophic lake. *Microb. Ecol.* **2003**, 46, 22–32; DOI
692 10.1007/s00248-002-1064-6

693 Hoffmann, A.; Gunkel, G. Bank filtration in the sandy littoral zone of Lake Tegel
694 (Berlin): Structure and dynamics of the biological active filter zone and clogging
695 processes. *Limnologica* **2011**, 41, 10–19; DOI 10.1016/j.limno.2009.12.003

696 Hua, G.; Zeng, Y.; Zhao, Z.; Cheng, K.; Chen, G. Applying a resting operation to
697 alleviate bioclogging in vertical flow constructed wetlands: an experimental lab
698 evaluation. *Journal of environmental management* **2014**, 136, 47-53.

699 Huettel, M.; Ziebis, W.; Forster, S.; Luther Iii, G. W. Advective transport affecting
700 metal and nutrient distributions and interfacial fluxes in permeable
701 sediments. *Geochimica et Cosmochimica Acta* **1998**, 62(4), 613-631.

702 Jeffrey, S. T.; Humphrey, G. F. New spectrophotometric equations for determining
703 chlorophylls a, b, c1 and c2 in higher plants, algae and natural
704 phytoplankton. *Biochemie und Physiologie der Pflanzen* **1975**, 167(2), 191-194.

705 Jeong, H. Y.; Jun, S. C.; Cheon, J. Y.; Park, M. A review on clogging mechanisms and
706 managements in aquifer storage and recovery (ASR) applications. *Geosciences*
707 *Journal* **2018**, 1-13.

708 Kia, A.; Wong, H. S.; Cheeseman, C. R. Defining clogging potential for permeable
709 concrete. *Journal of environmental management* **2018**, 220, 44-53.

710 Kim, J. W.; Choi, H.; Pachepsky, Y. A. Biofilm morphology as related to the porous

media clogging. *Water Research* **2010**, 44(4), 1193-1201.

Lappin-Scott, H. M.; Costerton, J. W. Bacterial biofilms and surface fouling. *Biofouling* **1989**, 1(4), 323-342.

Laspidou, C. S.; Rittmann, B. E. A unified theory for extracellular polymeric substances, soluble microbial products, and active and inert biomass. *Water Research* **2002**, 36(11), 2711–2720.

Li, Q. P.; Franks, P. J. S.; Landry, M. R.; Goericke, R., Taylor, A. G. Modeling phytoplankton growth rates and chlorophyll to carbon ratios in California coastal and pelagic ecosystems. *J. Geophys. Res. Biogeosciences* **2010**, 115, 1–12; DOI 10.1029/2009JG001111

Liu, Y.; Tay, J. H. The essential role of hydrodynamic shear force in the formation of biofilm and granular sludge. *Water research* **2002**, 36(7), 1653-1665.

Lock, M. A.; Wallace, R. R.; Costerton, J. W.; Ventullo, R. M.; Charlton, S. E. River epilithon: toward a structural-functional model. *Oikos* **1984**, 10-22.

Malarkey, J.; Baas, J. H.; Hope, J. A.; Aspden, R. J.; Parsons, D. R.; Peakall, J.; Paterson, D. M.; Schindler, R. J.; Ye, L.; Lichtman, I. D.; Bass, S. J.; Davies, A. G.; Manning, A. J.; Thorne, P. D. The pervasive role of biological cohesion in bedform development. *Nat. Commun*. **2015**, 6, 1–6; DOI 10.1038/ncomms7257

Margalef, R. *Limnología* (Vol. 1009); Omega: Barcelona, 1983

Mendoza-Lera, C.; Frossard, A.; Knie, M.; Federlein, L. L.; Gessner, M. O.; Mutz, M. Importance of advective mass transfer and sediment surface area for streambed microbial communities. *Freshwater Biology* **2017**, 62(1) 133–145; DOI 10.1111/fwb.12856

Mermillod-Blondin, F.; Mauclaire, L.; Montuelle, B. Use of slow filtration columns to assess oxygen respiration, consumption of dissolved organic carbon, nitrogen transformations, and microbial parameters in hyporheic sediments. *Water Res.* **2005**, 39, 1687–1698; DOI 10.1016/j.watres.2005.02.003

Meteocat - Meteorological Service of Catalonia Website. Department of Territory and Sustainability, Government of Catalonia. (Meteocat - Servei meteorològic de

Catalunya. Departament de Territori i Sostenibilitat, Generalitat de Catalunya). http://www.meteo.cat/wpweb/serveis/peticions-de-dades/peticio-dinformes-meteorologics (accessed Feb 12, 2017).

Miller, J. H.; Ela, W. P.; Lansey, K. E.; Chipello, P. L.; Arnold, R. G. Nitrogen Transformations during Soil–Aquifer Treatment of Wastewater Effluent—Oxygen Effects in Field Studies. *J. Environ. Eng.* **2009**, 132, 1298–1306; DOI 10.1061/ASCE0733-9372(2006)132:10(1298)

Nivala, J.; Knowles, P.; Dotro, G.; García, J.; Wallace, S. Clogging in subsurface-flow treatment wetlands: measurement, modeling and management. *Water research* **2012**, 46(6), 1625-1640.

Oberdorfer, J. A.; Peterson, F. L. Wastewater injection: geochemical and biogeochemical clogging processes. *Groundwater* **1985**, 23(6), 753-761.

Or, D.; Smets, B. F.; Wraith, J. M.; Dechesne, A.; Friedman, S. P. Physical constraints affecting bacterial habitats and activity in unsaturated phorous media – a review. *Adv. Water Resour.* **2007**, 30, 1505–1527; DOI 10.1016/j.advwatres.2006.05.025

Oyebamiji, O. K.; Wilkinson, D. J.; Jayathilake, P. G.; Rushton, S. P.; Bridgens, B.; Li, B.; Zuliani, P. A Bayesian approach to modelling the impact of hydrodynamic shear stress on biofilm deformation. *PloS one* **2018**, 13(4), e0195484.

Perujo, N.; Sanchez-Vila, X.; Proia, L.; Romaní, A. M. Interaction between Physical Heterogeneity and Microbial Processes in Subsurface Sediments : A Laboratory-Scale Column Experiment. *Environ. Sci. Technol*. **2017**, 51, 6110–6119; DOI 10.1021/acs.est.6b06506

Perujo, N.; Romaní, A. M.; Sanchez-Vila, X. Bilayer infiltration system combines benefits from both coarse and fine sands promoting nutrient accumulation in sediments and increasing removal rates. *Environ. Sci. Technol.* **2018**, 52(10), 5734-5743.

Pholkern, K.; Srisuk, K.; Grischek, T.; Soares, M.; Schäfer, S.; Archwichai, L.; Saraphirom, P.; Pavelic, P.; Wirojanagud, W. Riverbed clogging experiments at potential river bank filtration sites along the Ping River, Chiang Mai, Thailand. *Environmental Earth Sciences* **2015**, 73(12), 7699-7709.

Quéric, N. V.; Soltwedel, T.; Arntz, W. E. Application of a rapid direct viable count method to deep-sea sediment bacteria. *J. Microbiol. Methods* **2004**, 57, 351–367; DOI 10.1016/j.mimet.2004.02.005

Racz, A. J.; Fisher, A. T.; Schmidt, C. M.; Lockwood, B. S.; Huertos, M. L. Spatial and Temporal Infiltration Dynamics During Managed Aquifer Recharge. *Ground Water* **2012**, 50 (4), 562–570; DOI 10.1111/j.1745-6584.2011.00875.

Rodriguez-Escales, P.; Fernandez-Garcia, D.; Drechsel, J.; Folch, A.; Sanchez-Vila, X. Improving degradation of emerging organic compounds by applying chaotic advection in Managed Aquifer Recharge in randomly heterogeneous porous media. *Water Resources Research* **2017**, 53 (5), 4376-4392

Rubol, S.; Freixa, A.; Carles Brangari, A.; Fernandez-Garcia, D.; Romani, A. M.; Sanchez-Vila, X. Connecting bacterial colonization to physical and biochemical changes in a sand box infiltration experiment. *Journal of hydrology* **2014**, 517, 317-327; DOI 10.1016/j.jhydrol.2014.05.041.

Santmire, J. A.; Leff, L. G. The influence of stream sediment particle size on bacterial abundance and community composition. *Aquatic Ecology* **2007**, 41(2), 153-160.

Segismundo, E. Q.; Kim, L. H.; Jeong, S. M.; Lee, B. S. A laboratory study on the filtration and clogging of the sand-bottom ash mixture for stormwater infiltration filter media. *Water* **2017**, 9(1), 32.

Stoodley, P.; Sauer, K.; Davies, D. G.; Costerton, J. W. Biofilms as complex differentiated communities. *Annu. Rev. Microbiol*. **2002**, 56, 187–209; DOI 10.1146/annurev.micro.56.012302.160705

Tang, Q.; Gu, F.; Zhang, Y.; Zhang, Y.; Mo, J. Impact of biological clogging on the barrier performance of landfill liners. *Journal of environmental management* **2018**, 222, 44-53.

Thullner, M.; Zeyer, J.; Kinzelbach, W. Influence of Microbial Growth on Hydraulic Properties of Pore Networks. *Transp. Porous Media* **2002**, 49, 99–122.

Thullner, M. Comparison of bioclogging effects in saturated porous media within one- and two-dimensional flow systems. *Ecological Engineering* **2010**, 36(2), 176-196.

Türkmen, M.; Walther, E. F.; Andres, A. S.; Chirnside, A. A. E.; Ritter, W. F. Evaluation of rapid infiltration basin systems (RIBS) for wastewater disposal: Phase I. *Delaware Geol. Surv.* **2008**.

Vandevivere, P.; Baveye, P. Effect of bacterial extracellular polymers on the saturated hydraulic conductivity of sand Effect of Bacterial Extracellular Polymers on the Saturated Hydraulic Conductivity of Sand Columns. *Appl. Envirnomental Microbiol.* **1992**, 58, 1690–1698.

Vivas, Z.; Perujo, N.; Freixa, A.; Romaní, A. M. Changes in bacterioplankton density and viability in the Tordera river due to the input of effluents from waste water treatment plants. *Limnetica* **2017**, 36, 461–475; DOI 10.23818/limn.36.15

Watnick, P. I.; Kolter, R. Steps in the development of a Vibrio cholerae El Tor biofilm. *Molecular microbiology* **1999**, 34(3), 586-595.

Xia, L.; Zheng, X.; Shao, H.; Xin, J.; Peng, T. Influences of environmental factors on bacterial extracellular polymeric substances production in porous media. *J. Hydrol.* **2014**, 519, 3153–3162; DOI 10.1016/j.jhydrol.2014.10.045

Xia, L.; Zheng, X.; Shao, H.; Xin, J.; Sun, Z.; Wang, L. Effects of bacterial cells and two types of extracellular polymers on bioclogging of sand columns. *J. Hydrol.* **2016**, 535, 293–300; DOI 10.1016/j.jhydrol.2016.01.075

Yan, Z.; Liu, C.; Liu, Y.; Bailey, V. L. Multiscale Investigation on Biofilm Distribution and Its Impact on Macroscopic Biogeochemical Reaction Rates. *Water Resour. Res.* **2017**, 53, 8698–8714; DOI 10.1002/2017WR020570

Zhong, H.; Liu, G.; Jiang, Y.; Yang, J.; Liu, Y.; Yang, X.; Liu, Z.; Zeng, G.. Transport of bacteria in porous media and its enhancement by surfactants for bioaugmentation: A review. *Biotechnol. Adv*. **2017**, 35, 490–504; DOI 10.1016/j.biotechadv.2017.03.009

Zhong, X.; Wu, Y. Bioclogging in porous media under continuous-flow condition. *Environmental earth sciences* **2013**, 68(8), 2417-2425.

Zhou, Y.; Luo, S.; Yu, B.; Zhang, T.; Li, J.; Zhang, Y. A comparative analysis for the development and recovery processes of different types of clogging in lab-scale

vertical flow constructed wetlands. *Environmental Science and Pollution Research* **2018**, 25(24), 24073-24083.